

Inverting the Diastereoselectivity of the Mukaiyama–Michael Addition with Graphite-Based Catalysts

Maria Rosaria Acocella,^{*,†} Marco Mauro,[†] Laura Falivene,[†] Luigi Cavallo,^{*,‡} and Gaetano Guerra^{*,†}

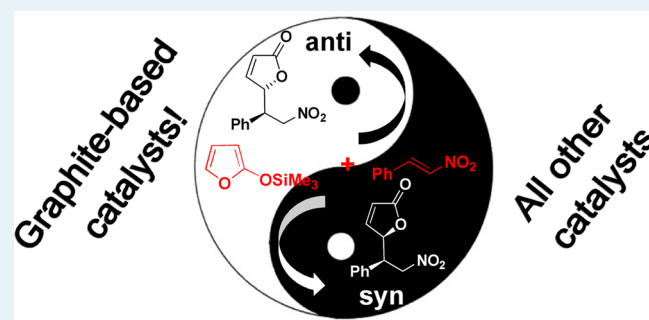
[†]Department of Chemistry and Biology and INSTM Research Unit, Università di Salerno, via Giovanni Paolo II, 84084 Fisciano, Italy

[‡]KAUST Catalysis Center, King Abdullah University of Science & Technology, Thuwal 23955-6900, Kingdom of Saudi Arabia

Supporting Information

ABSTRACT: Here, we show that graphite-based catalysts, mainly graphite oxide (GO) and exfoliated GO, are effective recyclable catalysts for a relevant stereoselective Mukaiyama–Michael addition, outperforming currently available catalysts. Moreover, the graphite-based catalysts described here invert the diastereoselectivity relative to that observed with known catalysts, with the unprecedented large prevalence of the *anti* diastereoisomer. This inverted diastereoselectivity is increased when the catalyst concentration is reduced and after catalyst recycling. Density functional theory calculations suggest that the selectivity is determined by two types of supramolecular interactions operating between the catalyst and the substrates at the diastereoselectivity-determining transition state, specifically, the π -stacking of β -nitrostyrene with graphite and the van der Waals interaction between the SiMe₃ group of the silyl ether and the graphite.

KEYWORDS: carbocatalysis, Mukaiyama–Michael addition, inversion of diastereoselectivity, graphite-based catalysts, solvent-free

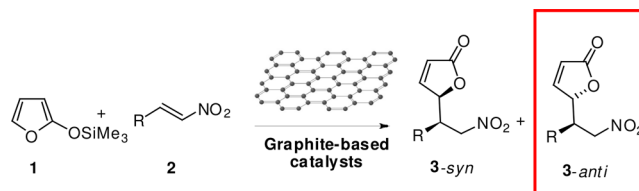


INTRODUCTION

The need for sustainable and metal-free catalytic processes has stimulated the development of carbocatalysis,¹ through which synthetic transformations are promoted by carbon-based materials. In particular, graphite oxide (GO)² and exfoliated graphite oxide (eGO, also called graphene oxide), but also in many cases high-surface area graphite and graphene, have been shown to have relevant catalytic activity in oxidations,³ Friedel–Crafts⁴ or aza-Michael additions,⁵ and polymerizations.^{6,7} Graphite-based catalysts have many advantages, including being heterogeneous, environmentally benign, and inexpensive. However, the main drawback of graphite-based catalysts is that very high catalyst loading is generally needed, which for many reactions is in the range of 50–200 wt % with respect to the substrate.¹ An additional inconvenience is the generally poor selectivity of the catalyzed reactions. In this paper, we show that graphite-based samples (mainly when oxidized) are highly effective as catalysts for the asymmetric Mukaiyama–Michael addition of 2-(trimethylsilyloxy)furan (TMSOF) to a family of β -nitroalkenes (see Scheme 1).

The products of this reaction, functionalized butenolides, are important intermediates for the synthesis of natural⁸ and biologically active compounds,⁹ because of the presence of the nitro group, which makes them easily manipulated (for example, through the Nef reaction,¹⁰ the Meyer reaction,¹¹ and reduction to the amino group¹²). Moreover, for the first time, we show not only that graphite-based catalysts are chemically selective but also that their selectivity is inverted with respect to the selectivity of traditional homogeneous and

Scheme 1. Stereoselective Mukaiyama–Michael Addition of 2-(Trimethylsilyloxy)furan to β -Nitroalkenes



heterogeneous catalysts. In particular, a large prevalence of the *anti* diastereoisomer, which is a minor product of this reaction when it is catalyzed by traditional catalysts, is obtained with graphite-based catalysts.

RESULTS AND DISCUSSION

One of the graphite samples used in this paper is a high-surface area (308 m²/g) graphite, whose X-ray diffraction pattern is shown in Figure 1A.¹³ This pattern shows narrow 002, 100, and 110 reflections, corresponding to long-range order that is both perpendicular ($D_{002} = 10$ nm) and mainly parallel to the graphitic planes ($D_{100} > 30$ nm).¹³

GO and eGO samples used in this paper were prepared by Hummers' oxidation^{2b} of the graphite samples of Figure 1A and

Received: November 12, 2013

Revised: December 19, 2013

Published: December 27, 2013

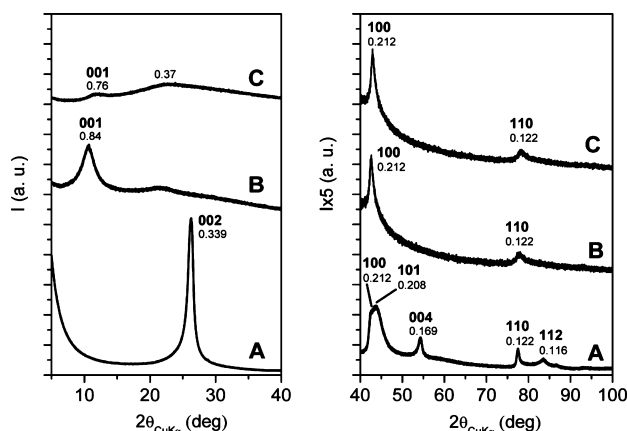


Figure 1. X-ray diffraction patterns (Cu K α) of the starting graphite (A), the derived GO (B), and eGO (C). GO and eGO essentially maintain the crystalline order parallel to the graphitic layers ($D_{100} > 30$ nm).

present the X-ray diffraction patterns shown in parts B and C of Figure 1. These X-ray diffraction patterns show the maintenance of the 100 and 110 reflections and the disappearance of the periodicity perpendicular to the graphite layers (002 and 004 reflections). These reflections are replaced by a broad reflection with a spacing d of 0.84 nm and a correlation length D of ≈ 4.5 nm (Figure 1B), corresponding to the 001 reflection of GO.^{14–16} For the milled graphite oxide sample in Figure 1C, this reflection is nearly completely replaced by a very broad intense halo, centered at a d of 0.37 nm with a correlation length of ~ 1 nm, indicating the presence of a large fraction of essentially exfoliated GO.¹⁷ Our GO and eGO samples have similar C/O ratios (nearly 1.7, according to elemental analyses) and largely different surface areas (according to BET measurements): 0.8 and 4.6 m²/g, respectively. These surface area values agree well with those reported in the literature for GO samples,^{6,18,19} while they are definitely lower than the value for starting graphite.

The powders characterized in Figure 1 were used as possible catalysts for the Mukaiyama–Michael addition of TMSOF **1** to β -nitrostyrene **2a**, chosen as a representative substrate (see Table 1). In the absence of a catalyst, under solvent-free conditions, the reaction has a low yield and poor diastereoselectivity in favor of the *syn* adduct (Table 1, entry 1). The reaction, again under solvent-free conditions, is improved with a high loading of Brønsted acids (typically 12 wt % with respect to nitrostyrene), leading to much higher yields. In particular, by using racemic BINOL phosphoric acid (BINOL-PA) and conducting the reaction at low temperatures, we found the *syn* selectivity is further increased [at -20 °C, the *syn/anti* ratio is 75/25 (Table 1, entry 2)].²⁰ Even higher *syn* selectivity (*syn/anti* ratio of 10/1) occurs with high loading (>50 wt % with respect to β -nitrostyrene) of organometallic compounds (dinuclear zinc complex dissolved in THF).²¹

The Mukaiyama–Michael addition of **1** to **2a** is much more efficient with a graphite-based catalyst. In fact, in the presence of a high GO loading (12 wt %), the reaction proceeds very efficiently at room temperature but with a poor *syn* selectivity (Table 1, entry 3). Lowering the GO loading to the range of 0.2–2 wt % maintains good yields, while a surprisingly and unprecedented selectivity in favor of the *anti* diastereoisomer is observed (Table 1, entries 4 and 5)

Table 1. Stereoselective Mukaiyama–Michael Addition of **1** to **2a** under Solvent-Free Conditions

entry	catalyst (wt %)	T (°C) ^a /t (h)	yield (%) ^b	dr (<i>syn/anti</i>) ^c
1	–	rt/1.5	12	57/43
2	BINOL-PA (12)	$-20/6$	82	75/25
3	GO (12)	rt/3	90	59/41
4	GO (2)	rt/5	95	25/75
5	GO (0.2)	rt/6	85	25/75
6	GO (0.2)	$-20/20$	75	38/62
7	eGO (0.2)	rt/6	90	23/77
8	eGO (0.02)	rt/24	60	20/80
9	HSAG (0.2) ^d	rt/18	60	27/73
10	carbon black (0.2)	rt/6	68	24/76

^art means room temperature. ^bAll yields refer to isolated chromatographically pure compounds. ^cThe diastereoisomeric ratio (dr) was determined by ¹H nuclear magnetic resonance analysis (400 MHz) of the crude products. ^dThe reaction was performed with the high-surface area graphite of Figure 1a.

This catalytic activity with inverted diastereoselectivity is captured in the nuclear magnetic resonance (NMR) spectra shown in Figure 2, where the peaks of the *anti*-**3a** diastereoisomer at 5.20 ppm become prominent with respect to those of the *syn*-**3a** diastereoisomer at 5.37 ppm. This *anti* selectivity is not improved by lowering the reaction temperature or by performing the reaction in DCM. The use of eGO further improves the yield for 0.2 wt % (cf. entries 5 and 7 of Table 1, from 85 to 90%) and also the *anti* selectivity up to a diastereoisomeric ratio of 20/80 with a catalytic amount of 0.02 wt % (Table 1, entry 8), both possibly associated with the higher surface area.

We also screened the catalytic activity of less oxidized graphitic materials, such as the graphite oxide after reduction with ascorbic acid and carbon black (with C/O ratios nearly equal to 5 and 30, respectively) as well as the high-surface area graphite shown in Figure 1A (Table 1, entry 8). For these graphite-based catalysts, we observed *syn/anti* selectivity not far from 25/75, although the reaction yields were reduced to 65–70%. It is worth adding that structurally ordered graphite samples (with surface areas of <20 m²/g) have yields of $<60\%$ and poor diastereoselectivity. When taken together, the data in Table 1 indicate that the essential features leading to *anti* selectivity are present in single graphite layers.

Density functional theory (DFT) calculations were performed to shed light on the origin of the diastereoselectivity in the systems reported in Table 1. To this end, we focused on the diastereoselective-determining C–C bond formation step in the uncatalyzed and BINOL-PA-catalyzed reaction on one side and the graphite-catalyzed reaction on the other. To model graphite, we considered a sheet with 54 C atoms, consisting of 19 fused six-membered rings, and to model BINOL-PA, we used a biphenyl linker (see the Supporting Information). The difference in energy between the diastereoselective transition states leading to the *syn* and *anti* products, $\Delta E_{syn-anti}$ is used to gauge the diastereoselectivity of the reaction. Positive or negative values of $\Delta E_{syn-anti}$ indicate that formation of the *anti*

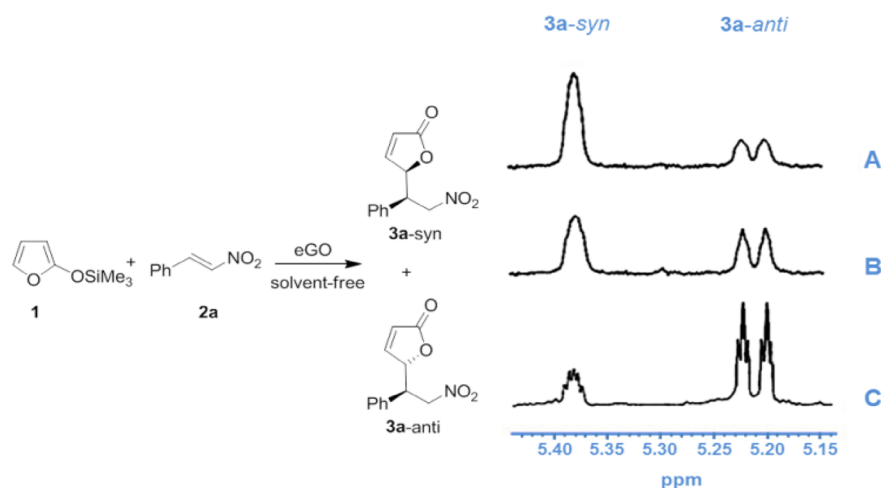


Figure 2. ^1H NMR spectra in the 5.45–5.15 ppm region of the **3a** products refer to the stereocenters of the butenolide core: (A) with 12 wt % BINOL-PA at $-20\text{ }^\circ\text{C}$ at a *syn/anti* ratio of 75/25, (B) with 12 wt % GO at room temperature with a *syn/anti* ratio of 59/41, and (C) with 0.2 wt % GO at room temperature with a *syn/anti* ratio of 25/75. The inverted diastereoselectivity in the presence of a catalytic amount of GO is clearly apparent.

or *syn* product, respectively, is favored. According to our calculations, $\Delta E_{\text{syn-anti}}$ values of -1.7 and -3.0 kcal/mol were obtained for the uncatalyzed reaction and for the reaction catalyzed by BINOL-PA, respectively, while a $\Delta E_{\text{syn-anti}}$ of 4.2 kcal/mol was obtained for graphite. These results indicate that the calculations could reproduce the inversion of the diastereoselectivity observed experimentally, and thus, they can be used to reveal the origin of the peculiar behavior exhibited by graphite-based catalysts. The geometry of the transition states reported in Figure 3 indicates that the β -nitrostyrene molecule is engaged in a π -stacking interaction with the graphite layer. Because of this interaction, TMSOF can attack the activated β -nitrostyrene only from the top. The main difference between the two transition states is in the relative orientation of TMSOF, which is engaged in a series of dispersive interactions with the C atoms of the graphite in the *anti* transition state (see the short distances in Figure 3A), because the SiMe_3 group protrudes away from the reactants. In contrast, in the *syn* transition state, the SiMe_3 group is basically oriented above the NO_2 group of β -nitrostyrene, and only weak interactions can occur with the graphite layer, as indicated by a distance of $\geq 5\text{ \AA}$ (see Figure 3B). In the case of the uncatalyzed reaction, a favorable electrostatic interaction between the positively charged SiMe_3 group and the negatively charged nitro group instead drives the formation of the *syn* product due to the proximity of these groups in the *syn* transition state (roughly 3.5 \AA) compared with the distance in the *anti* transition state (roughly 5.5 \AA). Finally, in the case of the reaction catalyzed by BINOL-PA, the geometrical constraint imposed by the activating phosphoric group matches the geometry of the uncatalyzed *syn* transition state better, leading to the reduced deformation energy of the substrates relative to that of the *anti* transition state (see the Supporting Information for additional details).

In the reaction pathway up to the reaction intermediate corresponding to formation of the C–C bond, the first step corresponds to π -stacking of β -nitrostyrene on the graphite layer, with an increase in energy of 14.8 kcal/mol in our model. The reaction proceeds with the attack of TMSOF on the graphite–nitrostyrene adduct, with a barrier of only 8.8 kcal/mol in the case of the favored *anti* pathway. The intermediate

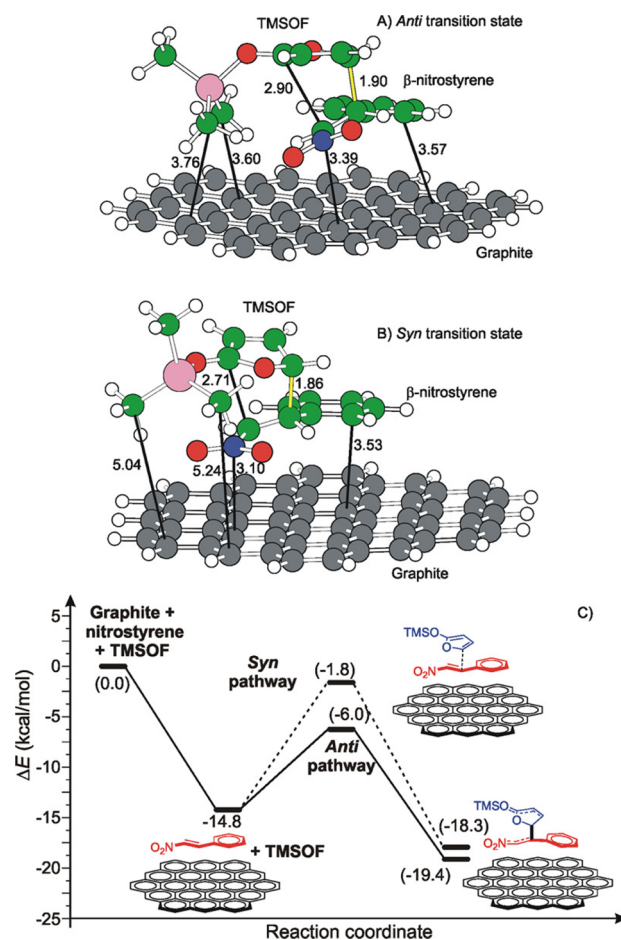


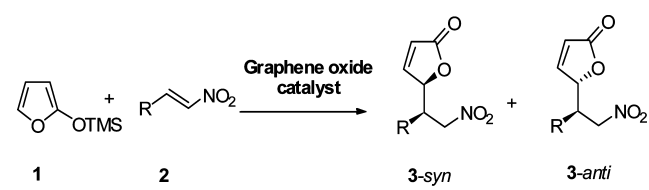
Figure 3. Geometry of the *anti* and *syn* transition states for the C–C bond-forming step in the presence of graphite (A and B). Distances are in angstroms. The C–C bond is colored yellow. (C) Energy profile up to the intermediate corresponding to the complete formation of the C–C bond.

with the fully formed C–C bond is only 4.6 kcal/mol more stable than the graphite–nitrostyrene adduct with the free TMSOF. Similar reaction profiles for the uncatalyzed and

BINOL-PA-catalyzed cases are described in the Supporting Information. The reaction of the addition intermediate with -OH groups always present in this kind of system leads to the liberation of the product. Because these steps do not have an impact on the diastereoselectivity, they were not considered here.

These results indicate that the observed catalytic activity and selectivity are possibly due to π -coordination of the reactant molecules with the graphite surfaces. To test this mechanistic hypothesis, we used nitroalkenes with no aromatic ring (Table 2, **2b** and **2c**) and a substrate with a more extended aromatic

Table 2. Stereoselective Mukaiyama–Michael Addition of TMSOF to Various Substituted β -Nitroalkenes



Entry	2	R	Time(h)	Yield (%) ^a	d.r. (<i>syn/anti</i>) ^b
1	2a		6	90	23/77
2	2b	-nC ₆ H ₁₃	24	/	/
3	2c		24	30	35/65
4	2d		24	65	15/85
5	2e		24	68	36/64
6	2f		24	23	31/69
7	2g		24	65	37/63
8	2h		24	73	41/59

^aAll yields refer to isolated chromatographically pure compounds.

^bThe diastereoisomeric ratio (dr) was determined by ¹H NMR analysis (400 MHz) of the crude products.

group (Table 2, **2d**). Consistent with the derived mechanistic scenario, the data reported in Table 2 indicate scarce or even no reactivity for substrates **2b** and **2c**, whereas there is increased selectivity with substrate **2d**, highlighting the fundamental role of the substrate–catalyst π -stacking interaction.

To assess the scope of the procedure, a variety of nitroalkenes was reacted with TMSOF under the conditions listed in entry 7 of Table 1. As reported in Table 2, the conjugate addition took place with moderate to good yields when the nitroalkenes had aromatic substituents in the β -position. The presence of an electron-donating group in the *para* position of the aromatic ring of β -nitrostyrene, as predicted, caused a remarkable decrease in efficiency (Table, 2, entry 6, substrate **f**), while a non-negligible reduction in the diastereoselectivity was detected with both electron-donating or -withdrawing groups (Table 2, entries 5–8, substrates **2e–2h**, respectively). As previously mentioned, the highest diastereoselectivity was achieved in the presence of a naphthyl group (Table 2, entry 4, substrate **2d**), whereas the lowest activity and selectivity were achieved with aliphatic nitroalkenes (Table 2, entries 2 and 3, substrates **2b** and **2c**, respectively), in agreement with our mechanistic hypothesis.

Finally, the reusability of GO was investigated using the addition of TMSOF to β -nitrostyrene **2a** as the model reaction.

The solid eGO, recovered after extraction from the aqueous solution and dried at 60 °C overnight, was used without any further treatment. The reaction conditions, room temperature and 6 h, were kept the same for all the cycles. As shown in Figure 4, the yield of the reaction remained almost unchanged

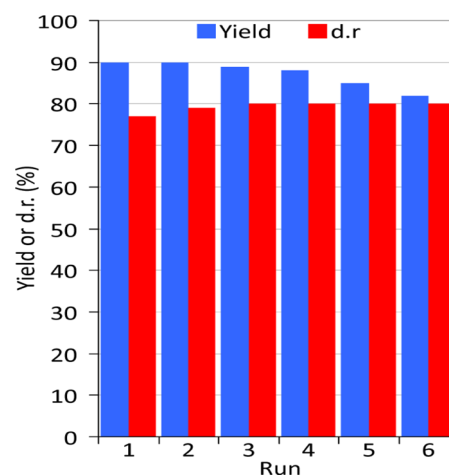


Figure 4. Yields (blue) and diastereoselectivity ratios (red) from the recycling experiments.

after five recycling steps, with only a reduction from 90 to 82%. In terms of the diastereoselectivity, a small improvement (*syn/anti* ratio of 20/80) was observed after the first cycle, and this improvement was preserved in the following cycles. These experiments suggest the remarkable recyclability of the catalyst using an extremely simple and economically convenient procedure. Further, the almost invariant yields and selectivity over several cycles indicate the heterogeneous nature of the catalyst, making it attractive for possible industrial applications.

CONCLUSION

We have shown that graphite-based materials (high-surface area graphite and carbon black), mainly when oxidized and exfoliated, are effective catalysts for the Mukaiyama–Michael addition of 2-(trimethylsiloxy)furan to β -nitroalkenes. They can operate under solvent-free conditions at a loading (0.02 wt %) much lower than those of catalysts presently described in the literature, which have to be used with much higher loadings (>10 wt %). Their heterogeneous and carbon-based nature makes them easily recyclable with almost unvaried performance after five cycles. The most relevant feature of these graphite-based catalysts is their unprecedented *anti* selectivity, replacing the usual *syn* selectivity of traditional catalysts. In short, we have described graphite-based catalysts (mainly exfoliated GO) that show inversion of the diastereoselectivity in favor of the *anti* isomer of the product, being also more effective and more economically and environmentally convenient than catalysts presently described in the literature.

DFT calculations and ad hoc experimental tests synergistically indicated the fundamental role of the catalyst, which engages with β -nitrostyrene in a stabilizing π -stacking interaction, while promoting *anti* selectivity through dispersive interactions with TMSOF. The high activity and inverted selectivity suggest the possibility of new applications in the field. Indeed, further studies are in progress to explore the catalytic activity and selectivity of graphite-based catalysts for other reactions.

EXPERIMENTAL SECTION

The reaction was conducted in a dry vial. Nitrostyrene (74.6 mg, 0.50 mmol) and 2-(trimethylsilyloxy)furan (101 μ L, 1.20 mmol) were added to the GO catalyst (0.2 wt %) at room temperature. The reaction mixture was stirred at the same temperature for the time indicated. The diastereoisomeric ratio was determined in a crude reaction by ^1H NMR. The reaction mixture was extracted with AcOEt, and the combined organic phase was dried (MgSO_4) and concentrated. The residue was purified by column chromatography on silica gel via gradient elution with petroleum ether/AcOEt to obtain the pure product. Graphite oxide samples were prepared by Hummers' method from graphite samples: 120 mL of sulfuric acid and 2.5 g of sodium nitrate were introduced into a 2000 mL three-neck round-bottom flask immersed in an ice bath, and 5 g of graphite was added, under nitrogen, with magnetic stirring. After a uniform dispersion of graphite powders had been obtained, 15 g of potassium permanganate was added very slowly to minimize the risk of explosion. The reaction mixture was thus heated to 35 $^\circ\text{C}$ and stirred for 24 h. The resulting dark green slurry was first poured into 6 L of deionized water and then centrifuged at 10000 rpm for 15 min in a Hermle Z 323 K centrifuge. The isolated GO powder was washed twice with 100 mL of a 5 wt % HCl aqueous solution and subsequently with deionized water. Finally, the powder was dried at 60 $^\circ\text{C}$ for 12 h.

All DFT static calculations were performed at the GGA level with the Gaussian09 set of programs. Geometry optimizations were performed using the M06 functional. The electronic configuration of the molecular systems was described with the standard split-valence basis set with a polarization function of Ahlrichs and co-workers for all atoms (the SVP keyword in Gaussian09). The geometry optimizations were performed without symmetry constraints, and the characterization of the located stationary points was performed by analytical frequency calculations. The reported energies were obtained via single-point energy calculations with the same functional and the triple- ζ basis set of Ahlrichs et al. on all atoms (the TZVP keyword in Gaussian09).

ASSOCIATED CONTENT

Supporting Information

Complete experimental procedures and characterization of products. This material is available free of charge via the Internet at <http://pubs.acs.org>.

AUTHOR INFORMATION

Corresponding Author

*E-mail: gguerra@unisa.it.

Notes

The authors declare no competing financial interests.

ACKNOWLEDGMENTS

We thank Prof. Arrigo Scettri, Dr. Marialuigia Raimondo, and Prof. Liberata Guadagno for useful discussions. The Ministero dell' Istruzione dell' Universit  e della Ricerca is gratefully acknowledged for financial support (PRIN).

DEDICATION

Dedicated to the 80th birthday of Prof. Adolfo Zambelli.

REFERENCES

- (1) Su, C.; Loh, K. P. *Acc. Chem. Res.* **2013**, *46*, 2275–2285.
- (2) (a) Staudenmaier, L. *Ber. Dtsch. Chem. Ges.* **1898**, *31*, 1481–1487. (b) Hummers, S. W. R.; Offeman, E. J. *Am. Chem. Soc.* **1958**, *80*, 1339.
- (3) (a) Mirza-Aghayan, M.; Kashef-Azar, E.; Boukherroub, R. *Tetrahedron Lett.* **2012**, *53*, 4962–4965. (b) Chu, X.; Zhu, Q.; Dai, W. L.; Fan, K. *RSC Adv.* **2012**, *2*, 7135–7139.
- (4) (a) Kumar, A. V.; Rao, K. R. *Tetrahedron Lett.* **2011**, *52*, 5188–5191. (b) Sarvari, M. H.; Slarghi, H. *Helv. Chim. Acta* **2005**, *88*, 2282–2287.
- (5) Verma, S.; Mungse, H. P.; Kumar, N.; Choudhary, S.; Jain, S. L.; Sain, B.; Khatri, O. P. *Chem. Commun.* **2011**, *47*, 12673–12675.
- (6) Dreyer, D. R.; Bielawski, C. W. *Adv. Funct. Mater.* **2012**, *12*, 3247–3253.
- (7) Dreyer, D. R.; Jarvis, K. A.; Ferreira, P. J.; Bielawski, C. W. *Macromolecules* **2011**, *44*, 7659–7667.
- (8) (a) Davis-Coleman, T.; Rivett, D. E. A. *Prog. Chem. Nat. Prod.* **1989**, *55*, 1–35. (b) Jefford, C. W.; Jaggi, D.; Sledeski, A. W.; Boukouvalas, J. In *Studies in Natural Products Chemistry*; Rahman, A., Ed.; Elsevier: Amsterdam, 1989; Vol. 3, p 157. (c) Paquette, L. A.; Wang, T. Z.; Pinard, E. J. *Am. Chem. Soc.* **1995**, *117*, 1455–1456. (d) Remoto, H.; Tanabe, T.; Fukumoto, K. *J. Org. Chem.* **1995**, *60*, 6785–6790.
- (9) (a) Fukui, H.; Tsuchiya, Y.; Fujita, K.; Nakagawa, T.; Koshino, H.; Nakata, T. *Biorg. Med. Chem. Lett.* **1997**, *7*, 2081–2086. (b) Uchida, T.; Fukui, H.; Tsuchiya, Y.; Fujita, K. JP Patent 100072468. (c) Hilborn, J. W.; Lu, Z.-H.; Jurgens, A. R.; Fang, Q. K.; Byers, P.; Wald, S. A.; Senanayake, C. H. *Tetrahedron Lett.* **2001**, *42*, 8919–8921.
- (10) For a review, see: Ballini, R.; Petrini, M. *Tetrahedron* **2004**, *60*, 1017–1047.
- (11) Kamlet, M. J.; Kaplan, L. A.; Dacons, J. C. *J. Org. Chem.* **1961**, *26*, 4371–4375.
- (12) (a) Beck, K.; Seebach, D. *Chem. Ber.* **1991**, *124*, 2897–2911. (b) Loyd, D. H.; Nichols, D. E. *J. Org. Chem.* **1986**, *51*, 4294–4295. (c) Barrett, A. G. M.; Spilling, C. D. *Tetrahedron Lett.* **1988**, *29*, 5733–5734. (d) Poupert, M. A.; Fazal, G.; Goulet, S.; Mat, L. T. *J. Org. Chem.* **1999**, *64*, 1356–1361.
- (13) (a) Mauro, M.; Cipolletti, V.; Galimberti, M.; Longo, P.; Guerra, G. *J. Phys. Chem. C* **2012**, *116*, 24809–24813. (b) Mauro, M.; Maggio, M.; Cipolletti, V.; Galimberti, M.; Longo, P.; Guerra, G. *Carbon* **2013**, *61*, 395–403.
- (14) Chen, D.; Zhu, H.; Liu, T. *ACS Appl. Mater. Interface* **2010**, *2*, 3702–3708.
- (15) Guo, Y.; Bao, C.; Song, L.; Yuan, B.; Hu, Y. *Ind. Eng. Chem. Res.* **2011**, *50*, 7772–7783.
- (16) (a) Zhang, S.; Shao, Y.; Liao, H.; Engelhard, M. H.; Yin, G.; Lin, Y. *ACS Nano* **2011**, *5*, 1785–1791. (b) Gao, W.; Alemany, L. B.; Ci, L.; Ajayan, P. M. *Nat. Chem.* **2009**, *1*, 403–408.
- (17) Jeon, I. Y.; Shin, Y. R.; Sohn, G. J.; Choi, H. J.; Bae, S. Y.; Mahmood, J.; Jung, S. M.; Seo, J. M.; Kim, M. J.; Chang, D. W.; Dai, L.; Baek, J. B. *Proc. Natl. Acad. Sci. U.S.A.* **2012**, *109*, 5588–5593.
- (18) Todd, A. D.; Bielawski, C. W. *Catal. Sci. Technol.* **2013**, *3*, 135–139.
- (19) Dreyer, D. R.; Murali, S.; Zhu, Y.; Ruoff, R. S.; Bielawski, C. W. *J. Mater. Chem.* **2011**, *21*, 3443–3447.
- (20) Scettri, A.; De Sio, V.; Villano, R.; Acocella, M. R. *Synlett* **2009**, *16*, 2629–2632.
- (21) Trost, B. M.; Hitce, J. J. *Am. Chem. Soc.* **2009**, *131*, 4572–4573.